Evaluation of Interpolation Kernels for SAR Interferometry

Ramon Hanssen and Richard Bamler

***Abstract*— Interpolation is required in interferometric synthetic aperture radar (SAR) processing for coregistration of complex signals. Straightforward system theoretical considerations provide objective figures of merit for interpolators, such as interferometric decorrelation and phase noise. Theoretical and simulation results are given for nearest neighbor, piecewise linear, four- and six-point cubic convolution, and truncated sinc kernels.**

***Index Terms*—Coherence, interpolation, phase errors, synthetic aperture radar (SAR) interferometry.**

I. Introduction

The first step in synthetic aperture radar (SAR) interferogram processing is often the resampling of one complex SAR image u_1 to map it onto a second image u_2 to within an accuracy of about a tenth of a resolution element.

Although the implementation may be different, resampling can be viewed as consisting of the following two steps:

1) reconstruction of the continuous signal from its sampled version by convolution with an interpolation kernel $i(x, y)$;
2) sampling of the reconstructed signal at the new sampling grid.

This scheme holds even in many cases in which the convolution [step 1] is not obvious. For example, nearest neighbor and Lagrange-type interpolation of equidistantly sampled data can be considered as a convolution with particular kernels. The choice of the interpolation kernel (especially its length) requires a tradeoff between interpolation accuracy and computational efficiency. This brief communications shows that straightforward system theoretical considerations give objective criteria for choosing or designing interpolation kernels for interferometric processing.

II. Theory of Interpolaration Errors

The following analysis starts from the classical Fourier domain description of interpolation errors in stationary signals. Often these errors are quantified in terms of an L^2 norm. We will instead employ coherence theory for SAR interferograms [1], [2] to predict the effect of interpolation on interferogram phase quality. Fig. 1 shows [for the one-dimensional (1-D) case] how the Fourier transform $I(f)$ of a kernel $i(x)$ acts as a transfer function on the periodically repeated signal power spectral density $|H(f)|^2$. The two classes of errors to be considered are the distortion of the useful spectral band $|f| \leq B/2$ and the insufficient suppression of its replicas $|f - nf_s||_{n\neq 0} \leq B/2$, where f_s is the sampling frequency. Hence, the interpolated signal will not be strictly low-pass limited and the subsequent new sampling creates aliasing terms. If in the resampling process all interpixel positions are equally probable, the aliasing terms are superposed incoherently and can be treated as noise with a signal to noise ratio of

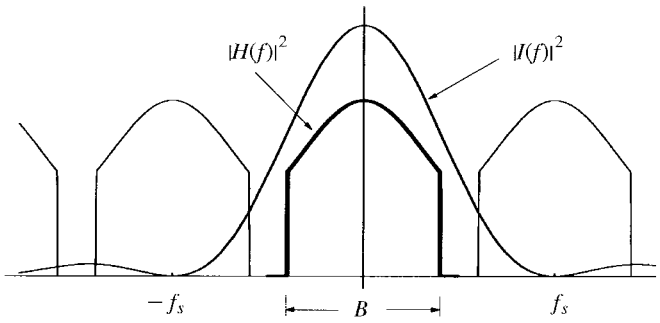

Fig. 1. Fourier transform $I(f)$ of interpolator $i(x)$ acting on the replicated signal spectrum.

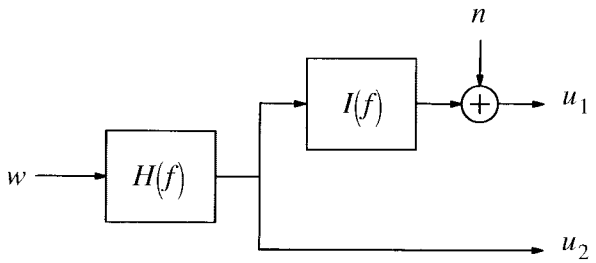

Fig. 2. System model for evaluating interpolation errors (w is a white circular Gaussian process).

$$\frac{S}{N} = \frac{\int_{-B/2}^{+B/2} |H(f)|^2 |I(f)|^2 \, df}{\sum_{n\neq 0} \int_{nf_s-B/2}^{nf_s+B/2} |H(f-nf_s)|^2 |I(f)|^2 \, df}. \tag{1}$$

In the following, we will quantify interpolation errors in terms of interferogram decorrelation and associated phase noise. We assume that the original data u_1 have been sampled at least at the Nyquist rate and the sampling distance after resampling is similar to the original.

The system model of Fig. 2 is sufficient for our analysis: consider a perfect and noise-free interferometric data pair of coherence $\gamma = 1$, before interpolation. Both u_1 and u_2 have passed the SAR imaging and processing system described by a transfer function $H(f)$. Signal u_1 additionally suffers from the interpolation transfer function $I(f)$ and alias noise n. It can be derived from [1] and [2] that, for circular Gaussian signals (i.e., for distributed targets), the coherence of such a system is given by

$$\gamma = \frac{1}{\sqrt{1 + \frac{N}{S}}} \cdot \frac{\int |H(f)|^2 I(f) \, df}{\sqrt{\int |H(f)|^2 \, df \cdot \int |H(f)|^2 |I(f)|^2 \, df}}. \tag{2}$$

These equations are readily extended to two dimensions. If both $H(f_x, f_y)$ and $I(f_x, f_y)$ are separable, we find

$$\gamma = \gamma_x \cdot \gamma_y. \tag{3}$$

The phase noise resulting from $\gamma < 1$ is known to be (in the N-look case)

$$\sigma_\phi^2 = \int_{-\pi}^{+\pi} \phi^2 \ \text{pdf}\,(\phi)\, d\phi \tag{4}$$

Manuscript received February 12, 1997; revised December 2, 1997.

R. Hanssen is with the Delft Institute for Earth Oriented Space Research (DEOS), Delft University of Technology, 2600 JA Delft, The Netherlands (e-mail: hanssen@geo.tudelft.nl).

R. Bamler is with the German Aerospace Research Establishment (DLR), German Remote Sensing Data Center, Oberpfaffenhofen, D-82234 Wessling, Germany (e-mail: Richard.Bamler@dlr.de).

Publisher Item Identifier S 0196-2892(99)00023-6.

TABLE I
THEORETICALLY AND SIMULATION-DERIVED INFLUENCE OF DIFFERENT 1-D AND 2-D INTERPOLATORS ON INTERFEROGRAM COHERENCE AND PHASE NOISE (PHASE STANDARD DEVIATION WITHOUT MULTILOOKING)

	One- Dimensional				Two- Dimensional	
	Coherence		Phase [deg] std.		Coherence	Phase std. [deg]
	theory	simu	theory	simu	theory	theory
nearest neighbor	0.9132	0.9042	37.4	36.4	0.8345	48.7
piecewise linear	0.9773	0.9757	21.4	20.1	0.9551	28.5
4-point cubic convolution	0.9949	0.9946	11.3	11.3	0.9898	15.2
6-point cubic convolution	—	0.9988	—	5.6	—	—
6-point truncated sinc	0.9975	0.9973	8.3	8.2	0.9950	11.2
8-point truncated sinc	0.9980	0.9979	7.4	7.0	0.9961	10.1
16-point truncated sinc	0.9995	0.9995	4.1	3.8	0.9990	5.6

where

$$\text{pdf}(\phi;\,\gamma,\,N) = \frac{\Gamma(N+1/2)(1-\gamma^2)^N\gamma\cos\phi}{2\sqrt{\pi}\Gamma(N)(1-\gamma^2\,\cos^2\,\phi)^{N+1/2}} + \frac{(1-\gamma^2)^N}{2\pi}\cdot {}_2F_1(N,\,1;\,1/2;\,\gamma^2\,\cos^2\,\phi) \quad (5)$$

and ${}_2F_1$ is the hypergeometric function.

III. EXAMPLES FOR INTERPOLARATORS

The interpolators and their spectra evaluated here are (assuming unity sample grid distance) [3], [4] as follows.

- Nearest neighbor:

$$i(x) = \text{rect}(x) = \begin{cases} 0, & |x| > \frac{1}{2} \\ \frac{1}{2}, & |x| = \frac{1}{2} \\ 1, & |x| < \frac{1}{2} \end{cases}$$
$$I(f) = \text{sinc}(f). \quad (6)$$

- Piecewise linear interpolation:

$$i(x) = \text{tri}(x) = \begin{cases} 0, & |x| > 1 \\ 1-|x|, & |x| < 1 \end{cases}$$
$$I(f) = \text{sinc}^2(f). \quad (7)$$

- Four-point cubic convolution ($\alpha = -1$):

$$i(x) = \begin{cases} (\alpha+2)|x|^3 - (\alpha+3)|x|^2 + 1, & 0 \le |x| < 1 \\ \alpha|x|^3 - 5\alpha|x|^2 + 8\alpha|x| - 4\alpha, & 1 \le |x| < 2 \\ 0, & 2 \le |x| \end{cases}$$
$$I(f) = \frac{3}{(\pi f)^2}\left[\text{sinc}^2(f) - \text{sinc}(2f)\right] + \frac{2a}{(\pi f)^2}\left[3\,\text{sinc}^2(2f) - 2\,\text{sinc}^2(2f) - \text{sinc}(4f)\right]. \quad (8)$$

- Six-point cubic convolution ($\alpha = -\frac{1}{2},\ \beta = \frac{1}{2}$):

$$i(x) = \begin{cases} (\alpha+\beta+2)|x|^3 - (\alpha+\beta+3)|x|^2 + 1 \\ \alpha|x|^3 - (5\alpha-\beta)|x|^2 + (8\alpha-3\beta)|x| - (4\alpha-2\beta) \\ \beta|x|^3 - 8\beta|x|^2 + 21\beta|x| - 18\beta \\ 0 \end{cases} \quad (9)$$

for $(0 \le |x| < 1)$, $(1 \le |x| < 2)$, $(2 \le |x| < 3)$, and $(3 \le |x|)$, respectively.

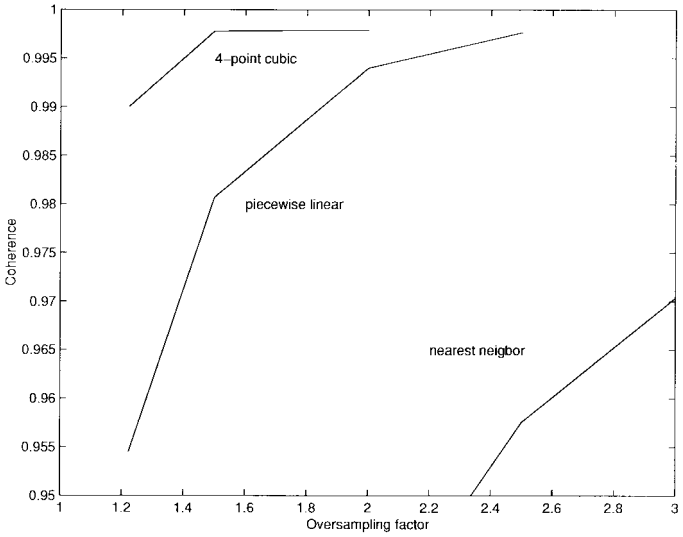

Fig. 3. Improvement of 2-D interpolation for oversampled input data (same oversampling factor in range and azimuth).

- Truncated sinc

$$i(x) = \text{sinc}(x)\,\text{rect}(x/L), \qquad \text{with } L = 6,\ 8,\ 16$$
$$I(f) = \frac{1}{\pi}\left(\text{Si}(\pi(f+0.5)L) - \text{Si}(\pi(f-0.5)L)\right) \quad (10)$$

where $\text{Si} = \int(\sin(x)/x)\,dx$.

Table I lists the theoretically derived coherence and one-look phase noise introduced by the first three and the last of these interpolators for one and two dimensions. ERS range signal parameters have been used for both dimensions with uniformly weighted spectrum and oversampling ratio of $f_s/B = 18.96$ MHz$/15.5$ MHz $= 1.223$ (in real systems, azimuth oversampling is slightly higher than in range), i.e., $H(f) = \text{rect}(f/B)$. Often, SAR data are oversampled by a higher factor before an interferogram is computed, be it either to avoid undersampling of the interferogram or as a consequence of baseline dependent spectral shift filtering. In these cases, the requirement on the interpolator is relaxed. Fig. 3 shows how decorrelation reduces with oversampling.

IV. EXPERIMENTAL RESULTS

Using uniformly distributed random generators R_i, a 1-D white circular Gaussian complex signal w is computed with amplitude $|w| = \sqrt{-\ln R_1[\cdot]}$ and phase $\arg(w) = 2\pi R_2[\cdot]$. Low-pass filtering yields a correlated random signal. An oversampling ratio of 12.23 is used to create the reference signal u, whereas the test signal u_s

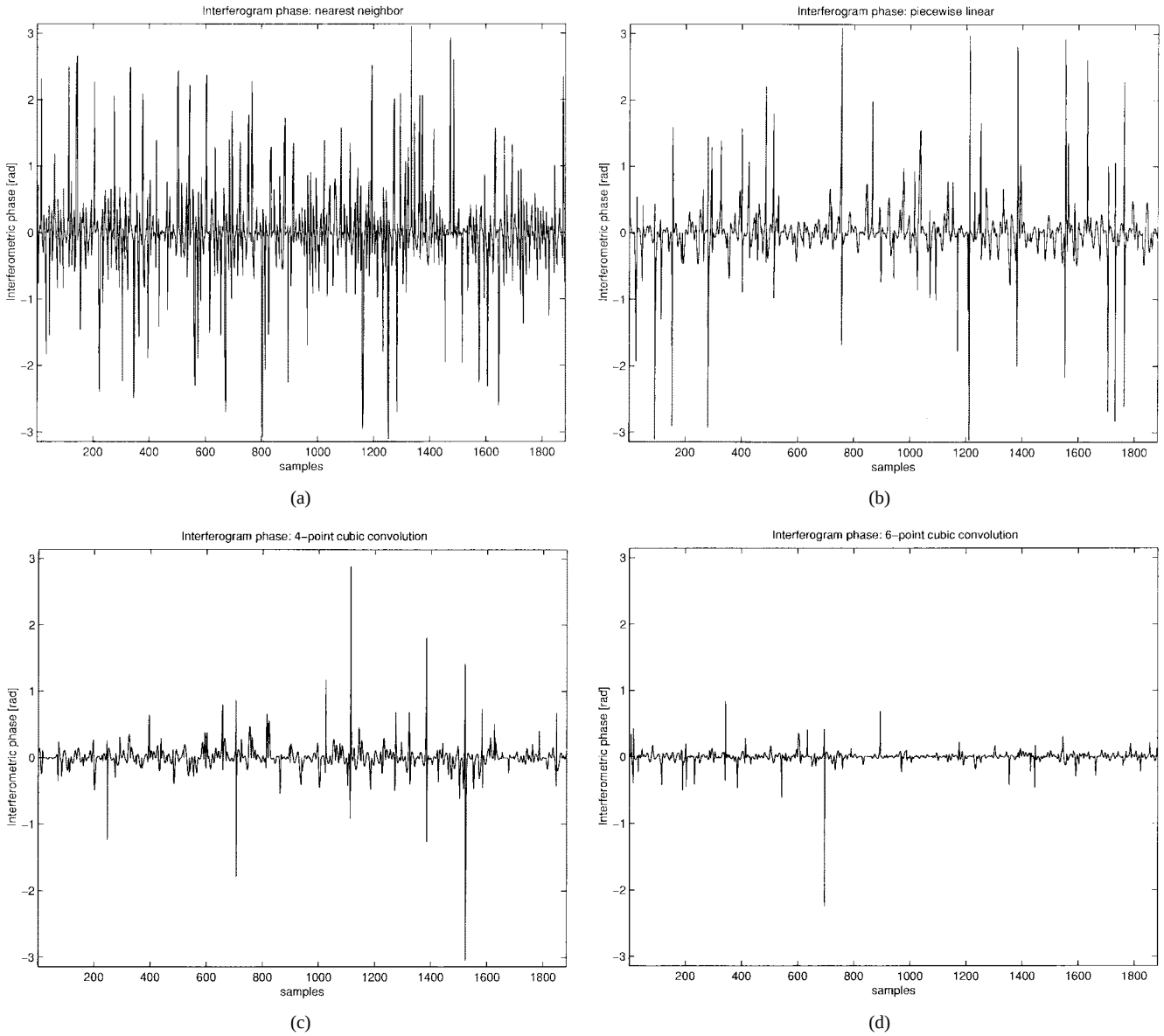

Fig. 4. Simulated interferograms using four kernels: (a) nearest neighbor, (b) piecewise linear, (c) four-point cubic convolution, and (d) six-point cubic convolution.

is a subsampled version thereof. Using a subsampling ratio of 1/10 reduces the oversampling ratio of the test signal to 1.223 to resemble ERS conditions. The test signal u_s is then interpolated using the kernels under investigation, yielding an estimate $\hat{u}$ of the reference signal. The interpolation kernels *nearest neighbor*, *piecewise linear*, *four-point* and *six-point cubic convolution*, and *six-point*, *eight-point*, and *16-point truncated sinc* are created using (6)–(10). For every kernel, the interferometric phase error $\phi = \arg[\hat{u} \cdot u^*]$, the phase error histogram, the total coherence γ, and the standard deviation of the interferometric phase error σ_ϕ are evaluated. Single experiment results of the interferometric phase error are shown for the first four evaluated kernels in Fig. 4. It can be seen that the variation of the interpolated signal decreases considerably as the kernel contains more sample points. Nevertheless, spurious spikes up to $\pm\pi$ still cause residues in the interferogram. The histogram is depicted in Fig. 5. The total coherence γ and the standard deviation of the interferometric phase σ_ϕ is studied using averaged values from 500 simulation loops. The results are given in Table I to allow comparison with the theoretical findings. Coherence has been estimated as the sample correlation coefficient of the reference signal u and the interpolated signal $\hat{u}$. Fig. 6 shows the mean standard deviation of the phase as a function of the coherence for the four shortest kernels.

V. Discussion of Results

The spurious spikes in the interferogram, as shown in Fig. 4, appear at those positions in the signal where the amplitude is extremely low. The signal to noise ratio at these interpolation points is therefore dominated by the interpolation noise. This makes a sudden phase jump at low-amplitude areas likely. Due to the small amplitude, multilooking suppresses these spikes and considerably diminishes the phase noise.

The cubic spline interpolation kernels used here can be referred to as parametric cubic convolution (PCC) [4]. The parameters α and β for the four- and six-point kernels chosen here have proved to be close to optimal for this particular configuration. Optimization for specific purposes can be performed by evaluating (1).

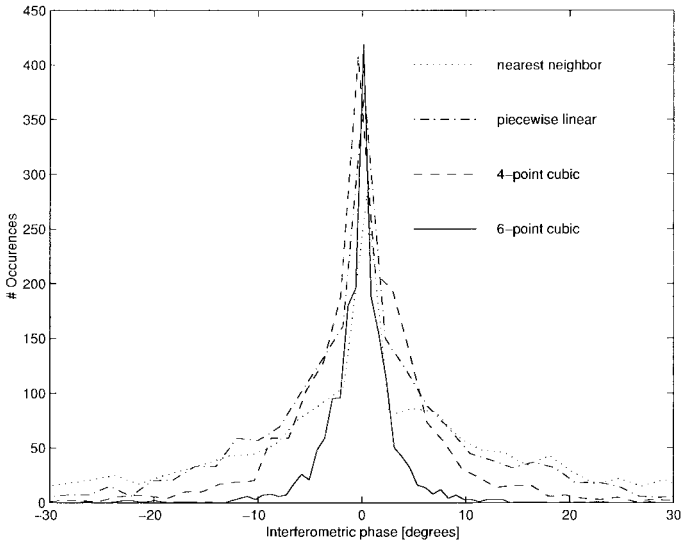

Fig. 5. Histogram of the phase errors for four kernels: nearest neighbor, piecewise linear, four-point cubic convolution, and six-point cubic convolution.

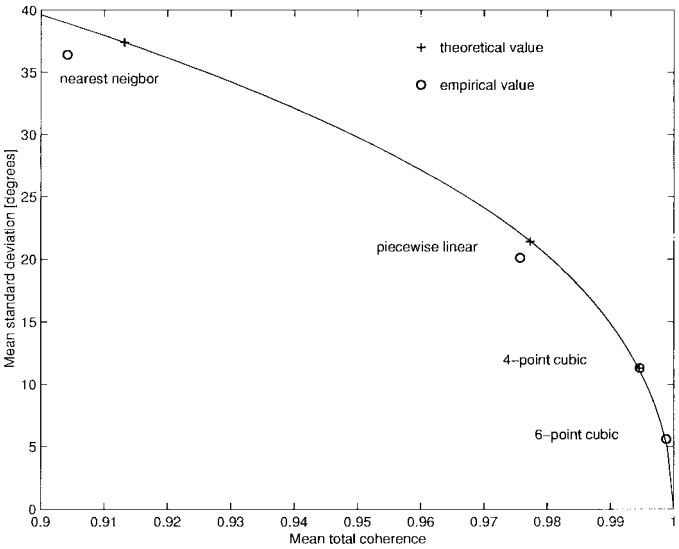

Fig. 6. Phase standard deviation phase and coherence for four interpolation kernels.

A comparison of cubic splines and truncated sincs underlines the necessity of careful interpolator design: note that the cubic splines used here are special cases of *weighted* truncated sincs. The six-point cubic convolution kernel showed better quality than an eight-point unweighted truncated sinc.

Interpolation errors are due to the aliasing of repeated signal spectra and the cutoff of the signal spectra's corners. Hence, the choice of an optimal interpolator will always depend on the correlation properties of the signal. However, a subjective recommendation can be given for ERS conditions, in which temporal decorrelation dominates the interferogram quality anyway. In these cases, a four-point cubic convolution with $\alpha = -1$ proved to be sufficient. For high-resolution applications of high-coherence single-pass interferometers, in which multilooking is not desirable, longer interpolation kernels, like the optimized six-point cubic convolution presented here, are recommended.

REFERENCES

[1] D. Just and R. Bamler, "Phase statistics of interferograms with applications to synthetic aperture radar," *Appl. Opt.*, vol. 33, no. 20, pp. 4361–4368, 1994.

[2] M. Cattabeni, A. Monti-Guarnieri, and F. Rocca, "Estimation and improvement of coherence in SAR interferograms," in *Proc. Int. Geosci. Remote Sensing Symp.*, Pasadena, CA, Aug. 8–12, 1994, pp. 720–722.

[3] R. G. Keys, "Cubic convolution interpolation for digital image processing," *IEEE Trans. Acoust., Speech, Signal Processing*, vol. ASSP-29, pp. 1153–1160, Dec. 1981.

[4] S. K. Park and R. A. Schowengerdt, "Image reconstruction by parametric cubic convolution," *Comput. Vision, Graph. Image Processing*, vol. 23, no. 3, pp. 258–272, Sept. 1983.